processes

MDPI

Article

Microwave Plasma-Driven Synthesis of Graphene and N-Graphene at a Gram Scale

Neli Bundaleska [1,*], Edgar Felizardo [1], Ana Dias [1], Ana Maria Ferraria [2,3], Ana Maria Botelho do Rego [2,3], Janez Zavašnik [4,5], Uros Cvelbar [4,5], Miroslav Abrashev [6], Jivko Kissovski [6], Amélia Almeida [7], Luís Lemos Alves [1], Bruno Gonçalves [1] and Elena Tatarova [1]

[1] Instituto de Plasmas e Fusão Nuclear, Instituto Superior Técnico, Universidade de Lisboa, 1049-001 Lisboa, Portugal; ines.vieitas@tecnico.ulisboa.pt (A.D.); bruno@ipfn.tecnico.ulisboa.pt (B.G.)
[2] Biospectroscopy and Interfaces Research Group, Institute for Bioengineering and Bioscence, Departamento de Engenharoa Quimica, Instituto Superior Técnico, Universidade de Lisboa, 1049-001 Lisboa, Portugal; amrego@tecnico.ulisboa.pt (A.M.B.d.R.)
[3] Associate Laboratory i4HB—Institute for Health and Bioeconomy at Instituto Superior Técnico, Universidade de Lisboa, 1049-001 Lisboa, Portugal
[4] Department of Gaseous Electronics F6, Jožef Stefan Institute, 1000 Ljubljana, Slovenia; uros.cvelbar@ijs.si (U.C.)
[5] Jožef Stefan International Postgraduate School, 1000 Ljubljana, Slovenia
[6] Faculty of Physics, Sofia University, 1164 Sofia, Bulgaria
[7] Centre of Physics and Engineering of Advanced Materials, Instituto Superior Técnico, Universidade de Lisboa, Av. Rovisco Pais 1, 1049-001 Lisboa, Portugal; amelia.almeida@tecnico.ulisboa.pt
* Correspondence: neli.bundaleska@ist.utl.pt

Academic Editors: Nikolay Yu. Peskov, Evgenia Benova and Frantisek Krcma

Received: 2 December 2024
Revised: 18 December 2024
Accepted: 10 January 2025
Published: 12 January 2025

Citation: Bundaleska, N.; Felizardo, E.; Dias, A.; Ferraria, A.M.; Botelho do Rego, A.M.; Zavašnik, J.; Cvelbar, U.; Abrashev, M.; Kissovski, J.; Almeida, A.; et al. Microwave Plasma-Driven Synthesis of Graphene and N-Graphene at a Gram Scale. *Processes* **2025**, *13*, 196. https://doi.org/10.3390/pr13010196

Correction Statement: This article has been republished with a minor change. The change does not affect the scientific content of the article and further details are available within the backmatter of the website version of this article.

Abstract: The large-scale microwave plasma synthesis of graphene and nitrogen-doped graphene with tailored structural properties, crucial for their successful usage applications, has been demonstrated. The developed atmospheric pressure plasma method offers several advantages, including the continuous production of high-quality, free-standing graphene without the use of chemicals, solvents, catalysts, or additional heating. This non-toxic process eliminates the need for vacuum systems while achieving high temperatures. The method enables the precise control over graphene's properties, such as the layer number, defects, sheet size, uniformity, and functionality, as well as the doping type and configuration, by adjusting the plasma parameters. Protocols for the synthesis of specific nanostructures with a controlled structural quality, production rate, and chemical composition have been established using methane and methylamine as precursors. The comprehensive physico-chemical characterization of the graphene and nitrogen-doped graphene was carried out using scanning electron microscopy, high-resolution transmission electron microscopy, Raman spectroscopy, X-ray diffraction, and X-ray photoelectron spectroscopy.

Keywords: plasma; graphene; nitrogen-doped graphene; atmospheric pressure; microwave plasma

1. Introduction

Graphene and graphene derivatives have received much scientific interest due to their unique combination of extraordinary properties. However, the industrial-scale production of these materials with a high purity, predefined properties, and moderate cost remains challenging. The graphene structural quality is essential for preserving its remarkable properties, i.e., the mechanical strength, electrical and thermal conductivities, chemical inertness, optical transparency, etc. In practice, the quality of graphene and derivative

products varies significantly, as it is highly dependent on the starting materials, manufacturing techniques, and fabrication condition monitoring, i.e., the control of the fabrication process [1,2].

The synthesis methods of graphene are categorized into two main approaches. Top-down methods, such as mechanical and chemical exfoliation, chemical syntheses, liquid-phase exfoliation (LPE), etc., employ the extraction of graphene from a bulk material, typically graphite. In contrast, bottom-up approaches, also known as construction techniques, are based on graphene assembling from atomic-scale carbon "building units", i.e., atoms, molecules, and radicals. The latter includes chemical vapor deposition (CVD), plasma-enhanced CVD (PECVD), epitaxial growth, and atmospheric pressure microwave plasma synthesis [3–9].

The manufacturing technology should ideally enable the control of the thickness, defect, uniformity, and contamination levels of the produced graphene material, corresponding to a standardized material. Another critical issue is the ability to scale-up the process while retaining the quality and properties of graphene, which typically rely on the synthesis equipment and parameters. Some of the developed processes, although providing high-value graphene (mechanical exfoliation, etc.) are laboratory-scale only. Considering the top-down approach, the characteristics of the final graphene product can also be affected by the starting graphite material, since it may have different morphologies, impurities, etc., depending on the supplier. Other critical points are the environmental effects, toxicity, and long-term stability. For instance, reduced graphene oxide (rGO) chemical production involves the use of large amounts of hazardous chemicals, such as nitric acid, sulfuric acid, sodium hydroxide, hydrazine, etc. [10]. Furthermore, the large volumes of water needed throughout the production of rGO can subsequently contain heavy metal ions and acids [11]. In addition to acids, in the LFE method, considerable quantities of a solvent are also required for the exfoliation process and to purify and disperse the exfoliated graphene sheets [12]. The recently developed method for "flash graphene" allows for a relatively high production yield, but it is intrinsically a batch process that is not fitted for continuous production, can only employ conductive solid carbons as starting materials, and requires post-treatment and suffers from electrode impurities, as evidenced by XRD analysis data [13].

The gas-phase synthesis of graphene and its derivatives using plasma is already an established method for continuous production, known as a technique that is able to control the high-temperature environment needed for attaining high-performance nanomaterials. Initial experiments of graphene synthesis were performed in atmospheric pressure microwave plasma by Dato et al. [14], with Ar plasma in a quartz tube and ethanol as a carbon precursor. Since then, several research groups have developed microwave plasma reactors and successfully synthesized graphene in a single-step and controllable manner [14–28].

The synthesis process involves the decomposition of an organic precursor in the "hot" reactive plasma medium to gas atoms and molecules, followed by their phase transformation into solid carbon in colder areas of the reactor. Selecting proper conditions, such as temperature gradients, the type and the amount of the precursor, the reactor design, as well as the residence time of the atoms and molecules in the plasma, promotes the synthesis of specific carbon nanomaterials (graphene, nanotubes, dots, etc.). The output material is in the form of free-standing nanostructures (substrate-free), which is the opposite to the other bottom-up approaches (pyrolysis, epitaxial growth, CVD, and PECVD), where the nanostructures are grown on the surface of a substrate [27–29]. The easy functionalization and modification of graphene is another advantage of the plasma method, resulting in materials with newly induced properties that are appropriate for specific applications. For instance, plasma-fabricated graphene hybrids, such as graphene-based metal oxide/sulfide

composites, are very interesting as catalysts and in different energy storage systems (fuel cells, lithium-ion batteries, Zn-air batteries, solar cells, and sensors) [30,31].

Herein, the microwave plasma process and the corresponding prototype working at atmospheric pressure for the continuous synthesis of free-standing graphene at a gram scale are presented. The same plasma approach was also used to achieve the in situ nitrogen doping of the graphene sheets during their assembly and growth in the "mild" plasma zone of the reactor. So far, protocols for the selective synthesis of graphene/N-graphene and graphene-based composites at a large scale have been established using ethanol, ethanol/methylamine, and acetonitrile as carbon/nitrogen precursors [31,32]. To further demonstrate the abilities and the versatile nature of the plasma prototype, we extended our investigations to precursors like methane and methylamine. The control of the type of doping was performed by changing the N-precursor injection position in the plasma environment, the flux of the precursors, and the residence time of growing the nanostructures. The microwave power and the precursor flux are parameters that significantly influence the thermal conditions in the plasma, and thus the nucleation and the growth of the carbon nanostructures. The present investigations include the synthesis process at different microwave powers and precursor flows, and their delivery positions. Additionally, the background gas was delivered either under laminar flow or swirl flow regimes. The protocols for the selective synthesis of graphene/N-graphene using methane/methylamine were determined [31–35].

2. Materials and Methods

2.1. Plasma Prototype

The plasma prototype, represented by 4 functional blocks, is shown in Figure 1. The first block consists of a microwave generator and waveguide components, such as a magnetron, a circulator, a stub set, a movable plunger, and a waveguide-surfatron [36]. The electromagnetic wave at 2.45 GHz emitted by the magnetron propagates in the TE mode. At the waveguide-surfatron, the propagation mode is converted to an azimuthally symmetric one, and an electromagnetic surface wave is launched along the reactor, in the interface between the reactor wall and the generated plasma. Thus, the plasma has an extension outside of the launcher zone, where large microwave power densities can be injected, and high population densities of the relevant active species can be achieved.

The second block includes the reactor tube, and the injection lines for the background gases and the precursors (comprising flow controllers (FCs), valves, gas cylinders, and the respective pressure reducers). The background gas was injected into the reactor from the top and close to the reactor's inner wall; the precursors were injected through smaller diameter quartz tubes, concentric with the reactor, one from the top (top-down injection) that passed through the region inside of the wave-launcher and terminated further down at the plasma's active zone; another from the bottom (bottom-up injection) that terminated at a mild plasma zone (Figure 1). This design permits control over the thermodynamic conditions (gas velocity, thermal fluxes, residence time, etc.) in the plasma reactor.

Block 3 encompasses the separation, collection, and filtering of the synthetized nanostructures. It consists of a chain of solid–gas separation elements—a tornado system with 2 to 5 containers for the collection of the synthesized solid material. A membrane filter collected the escaped particles, and the remaining gas was directed to a liquid trap before being exhausted. Water and air cooling systems ensured the proper continuous operation of the prototype from Block 4.

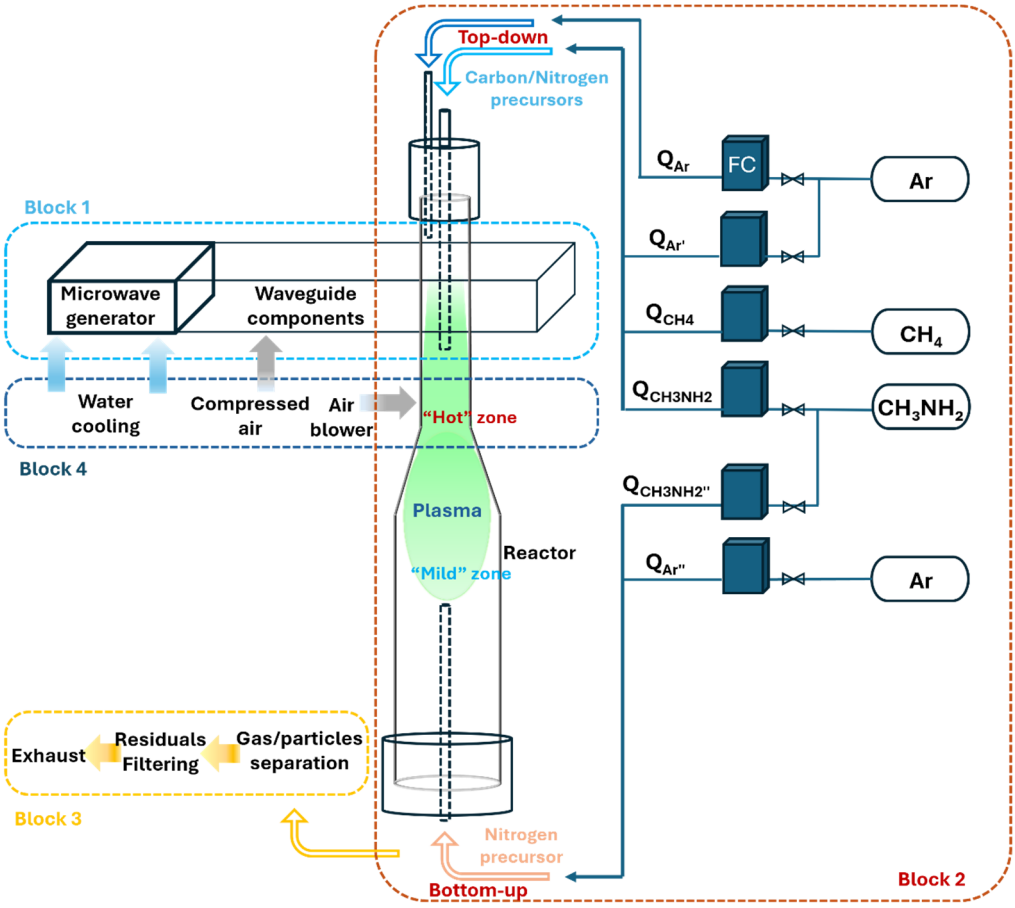

Figure 1. Schematic representation of the plasma prototype.

The plasma process of graphene formation, using a wide range of carbonaceous precursors, is described in detail elsewhere [31–35]. In brief, the plasma occupies two zones along the reactor tube, i.e., the "hot" zone maintained by the surface wave and the afterglow "mild" zone. In the "hot" zone, with temperatures up to ~ 4000 K, the precursor's molecules decompose due to collisions and intensified chemistry, leading to the formation of carbon atoms and molecules, among others (H, C_2H_2, C_2H_4, etc.) [33]. The newly created gas-phase carbon species involved in the formation of graphene, flowing with the background gas, pass through an isothermal surface (~2500 K), where their conversion into solid nuclei occurs. Further, they reach the "mild" zone (T~2000–500 K), where appropriate conditions for the assembly and growth of planar carbon nanostructures are intentionally established [31–35]. To achieve controllable N-graphene synthesis, the nitrogen precursor is also introduced into the plasma using the following two different configurations: top-down and bottom-up. The top-down scheme involves an injection of the nitrogen precursor (mixed with Ar gas, $Q_{Ar'}$) in the active "hot" zone together with the carbon precursor. In the bottom-up injection, the nitrogen precursor (mixed with Ar gas, $Q_{Ar''}$) is supplied from down into the "mild" plasma zone. The precursor flows both top-down and bottom-up were injected under laminar conditions.

2.2. Characterization Techniques

A Fourier transform infrared (FTIR) Thermo Nicolet 5700 spectrometer was used to investigate the 1000–4000 cm^{-1} absorption spectra of the species in the plasma outlet gas. For this purpose, a fraction of the output gas from the plasma reactor was probed at the bottom of the tube and directed to the FTIR spectrometer. The detection of species in the outlet gas flow stream was performed before and after the plasma was turned on.

Raman Spectroscopy analysis was performed using a LabRAM HR Visible (Horiba Jobin-Yvon) Raman spectrometer at 633 nm, with a 1 cm^{-1} spectral resolution and a laser spot size of 2 μm. The Raman spectra were taken from different regions of the synthesized nanostructures freely suspended on a glass substrate. Measurements were performed with a laser power P = 0.054 mW to avoid sample overheating.

The surface and morphology of the grown structures were analyzed by a Scanning Electron Microscope (SEM, the JSM-7001F, JEOL Inc., and the Helios NanoLab 650i, FEI Inc., Tokyo, Japan). The representative micrographs were acquired in the secondary electron imaging (SEI) mode at an accelerating voltage of 15 kV. The samples were then mounted by double-sided adhesive carbon tape on the aluminum stubs.

The morphology and crystal structure of the synthesized structures were analyzed by a Transmission Electron Microscope (TEM, the JEM-2010F, JEOL Inc., Tokyo, Japan) operating at 200 kV. The graphene flakes were transferred directly onto commercial copper-supported lacy carbon grids without further preparation. The nanoscale structures were visualized in conventional and phase-contrast (HR-TEM) modes, and micrographs were recorded by a slow-scan CCD camera (ORIUS SC1000, Gatan Inc., Pleasanton, CA, USA).

The crystal structure and phase composition of the synthesized structures were assessed by an X-ray diffractometer (XRD, D2 Phaser, Bruker Inc., Oeiras, Portugal) equipped with a CuKα source (wavelength λ = 0.154184 nm). The powdered samples were hand-pressed onto a zero-background sample holder to minimize the background signal. The tests were performed at room temperature in the scan range of 2θ = 5 to 95°. The data were acquired with a step size of 0.03° and an integration time/step of 5 s.

The X-ray photoelectron spectra (XPS) of the doped and undoped graphene were obtained with a non-monochromatic KRATOS XSAM800 dual-anode X-ray spectrometer (Kratos, San Diego, CA, USA). The Mg Kα X-radiation (1253.6 eV) was used. The binding energies (BEs) were corrected from the charge shift, taking as reference the binding energy of the sp^2 carbon atoms set at 284.4 eV. The quantification factors of the software library were used in the quantitative analysis. Other operation and acquisition conditions and data treatment details are published elsewhere [37].

3. Results

3.1. Plasma Characterization

The outlet gas stream FT-IR spectra detected for the investigated systems, i.e., graphene and N-graphene syntheses by using methane/methylamine as carbon/nitrogen precursors, respectively, are shown in Figure 2.

The absorption spectra were detected at the following conditions used for the graphene synthesis (Figure 2a): Q_{Ar} = 5.4 slm, $Q_{Ar'}$ = 2.07 slm, Q_{CH4} = 150 sccm, and P = 5.1 kW, with and without plasma. In both cases, the gas flow parameters were kept constant. The absorption spectrum detected without the plasma showed the characteristic for methane spectral lines at ~1300 and ~3000 cm^{-1} (C-H vibrations). When the plasma was turned on, these lines were absent, indicating that the carbon precursor molecules were completely decomposed in the hot plasma environment. The by-products detected are as follows: C_2H_2 (~750, 1300, and 3300 cm^{-1}), CO (asymmetrical vibrations at ~2170 cm^{-1}), and H_2 (detected by mass spectrometry). The spectra collected with the plasma on/off at operational conditions applied for N-graphene synthesis (Q_{Ar} = 5.4 slm, $Q_{Ar'}$ = 2 slm, Q_{CH4} = 150 sccm, Q_{Methyl} = 6 sccm, and P = 5.1 kW) are shown in Figure 2b. The spectrum collected without the plasma exhibited the methane spectral lines, as expected, as well as methylamine's fingerprint spectral region at 400–1500 cm^{-1} (the CH_3 antisymmetric stretch mode of CH_3NH_2 at around 2881 cm^{-1}, bands due to N-H vibrations at ~1650 to 1580 cm^{-1}, C-N vibrations at around 1020–1220 cm^{-1}, and C-H stretching vibrations at

around 2800–3000 cm^{-1}). These spectral lines disappeared when the plasma was turned on, and, simultaneously, the absorption peaks of C_2H_2, CO, and H_2 (mass spectrometry) were detected, demonstrating a complete decomposition of both of the precursors in the hot plasma environment. In fact, nearly 100% methane and methylamine conversion efficiencies were achieved in the plasma reactor.

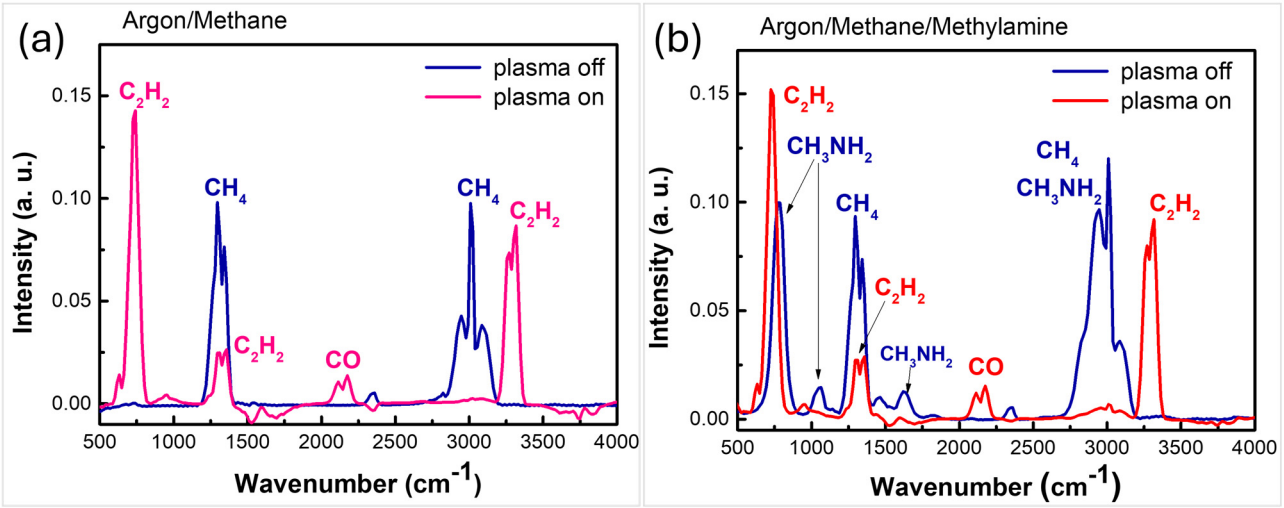

Figure 2. Infrared absorption spectra of the (**a**) Ar/methane and (**b**) Ar/methane/methylamine outlet gas with the plasma on and off.

3.2. Graphene Synthesis

To produce graphene, methane was used as a carbon precursor, delivered top-down, as shown in Figure 1, in two injection regimes of the background argon gas, i.e., the laminar and swirl. The following synthesis conditions of laminar injection flow were applied: #MG1: Q_{Ar} = 5.4 slm, $Q_{Ar''}$ = 2.07 slm, Q_{CH4} = 100 sccm, and P = 4.5 kW; #MG3: Q_{Ar} = 5.4 slm, $Q_{Ar'}$ = 2.07 slm, Q_{CH4} = 150 sccm, and P = 5.1 kW.

The samples synthesized under laminar flow conditions (#MG) revealed the dominant presence of small graphene-like sheets (~300 nm size), as seen on the SEM micrograph (Figure 3c). Moreover, the characteristic for the free-standing graphene morphology, comprising curved fine sheets, was revealed. The corresponding Raman spectra from three randomly chosen locations on the sample (#MG1), presented in Figure 3a, show three dominant Raman modes at ~ 1331, 1581, and 2657 cm^{-1}, attributed to the D-, G-, and 2D-bands, respectively. Additionally, low-intensity D′ (~1617 cm^{-1}), D+D″ (~2459 cm^{-1}), D+D′ (~2920 cm^{-1}), and 2D′ (~3238 cm^{-1}), typically observed in graphene-based structures, were also detected. The G-band is the intrinsic feature of all sp^2 carbon bonds. The D- and D′-bands are typically ascribed to defects, and their intensity depends on the concentration of the defects in the layer, as well as on the size of graphene flakes. The 2D-band, activated by a second-order scattering process, is the characteristic feature of the graphene. The high-intensity sharp 2D peaks in the Raman spectra (Figure 3a) provide evidence of the existence of single- and few-layer graphene sheets [33]. Moreover, the three spectra are nearly identical, indicating that the synthesized sample is homogeneous.

A significant difference in the 2D peaks is observed in the sample (#MG3). Increasing the methane flow and power supplied (Q_{CH4} = 150 sccm and P = 5.1 kW) leads to a decrease in the 2D peak intensity, indicating multilayer graphene synthesis. Keeping the lower value of the methane flow and the microwave power (Q_{CH4} = 100 sccm and P = 4.5 kW) results in the fabrication of single to multilayer graphene (Figure 3a,b). These results are consistent with our earlier observations [33]. Higher gas temperatures and lower precursor amounts promote the formation of fewer nucleation centers; thus, no supersaturation of the species

is possible. Such conditions promote the growth of already-existing nuclei rather than the creation of new ones, i.e., the growth into planar structures.

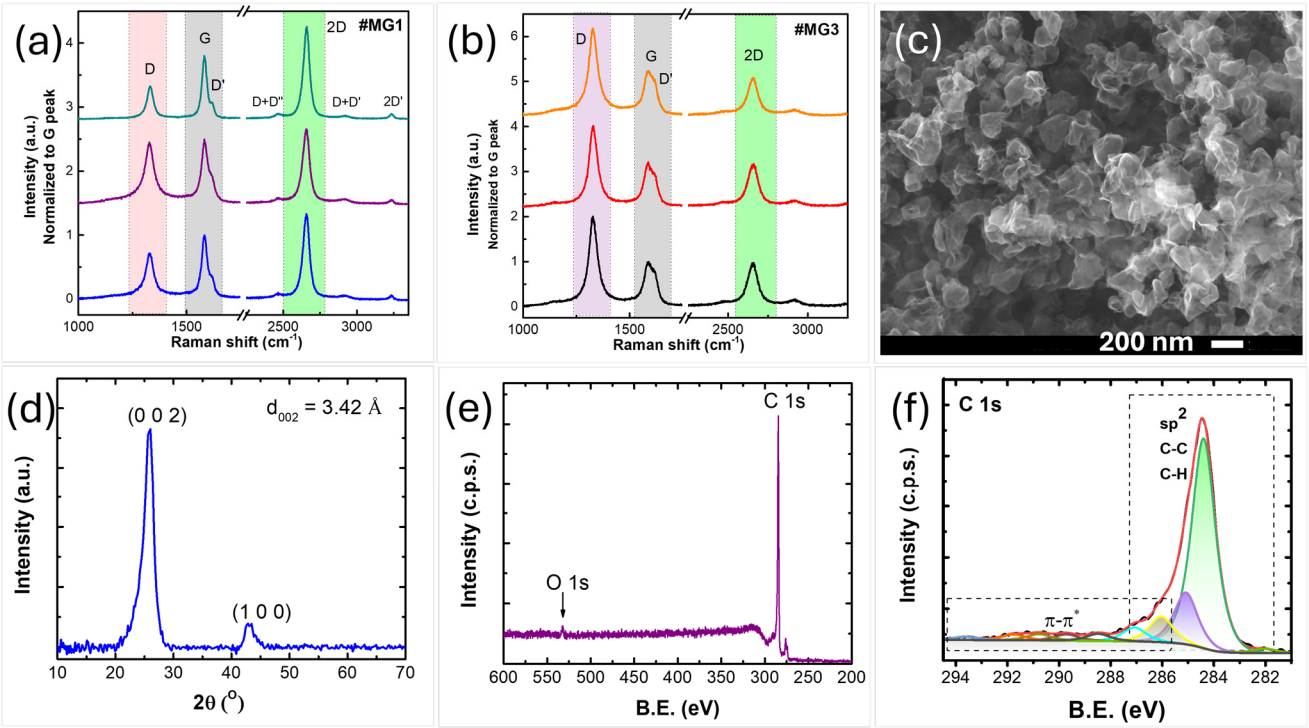

Figure 3. Raman spectra of (**a**) #MG1 (Q_{CH4} = 100 sccm) and (**b**) #MG3 (Q_{CH4} = 150 sccm) at randomly chosen locations, (**c**) the SEM, (**d**) the XRD pattern of the graphene fabricated with methane (Q_{CH4} = 150 sccm), (**e**) the XPS survey spectrum, and (**f**) the C 1s region of the graphene synthesized with methane (Q_{CH4} = 150 sccm). Synthesis conditions: #MG1 and #MG3.

The XRD pattern of the graphene sheets shows a well-defined (002) peak, implying successful graphitization (Figure 3d). The (002) peak occurs at a diffraction angle of 2θ = 26.04°, which corresponds to an interlayer spacing of 3.42 Å. This interlayer spacing is larger than that in a typical Bernal graphite (AB-stacked), at 3.37 Å, indicating the expanded and turbostratic structure of the synthesized graphene sheets [38]. The survey XPS spectra of the fabricated graphene sample (Q_{CH4} = 100 sccm) shows the C 1s and O 1s photoelectron regions (Figure 3e). The synthesized graphene has a relatively low level of oxidation (~3 at. O % and C/O ≈ 32.3). The XPS analysis of the C 1s region reveals the presence of planar structures, as evidenced by the high sp^2/C_{total} ≈ 63% (Figure 3f). Production yields ~10 mg/min (#MG1) and 15 mg/min (#MG3), which are higher than in the case of the ethanol precursor [35], have been achieved.

The following synthesis conditions under the swirl injection of the background gas flow were applied: #T8: Q_{Ar} = 9.4 slm, $Q_{Ar'}$ = 750 sccm, Q_{CH4} = 150 sccm, and P = 4.8 kW; #T22: Q_{Ar} = 9.4 slm, $Q_{Ar'}$ = 2 slm, Q_{CH4} = 150 sccm, and P = 4.8 kW. The results of their characterization are compared in Figure 4. The HRTEM images reveal the dominant presence of graphene-like sheets (Figure 4d,e). The corresponding Raman spectra (Figure 4a,b) show the three main features, namely, D, G, and 2D peaks, confirming their graphene nature. The spectra collected from different random locations of the sample #T8 (Figure 4a) are practically the same, indicating the synthesis of a homogeneous sample. By increasing the argon flux (injected along with the carbon precursor at the hot plasma zone), the synthesized structures of #T22 (Figure 4b) are no longer homogeneous, although few-layer graphene sheets are also present in the sample (the high-intensity 2D peak). The XRD patterns of both graphene samples show a pronounced graphitic (002) peak at

the diffraction angle of 2θ = 25.61°, which corresponds to an interlayer spacing of 3.47 Å (Figure 4c). Carbon and oxygen were identified in the survey XPS spectra (Figure 4f). The dominant contribution in the C 1s spectrum is attributed to sp^2 carbon, confirming the planar character of the nanostructures (Figure 4g,h). The XPS results demonstrate that graphene sheets were synthesized with a relatively low oxygen impurity, i.e., ~1.7% of O for #T8 and 2.1% of O % for #T22 (Figure 4i). The obtained production yield of the graphene sample #T8 is ~30 mg/min, which is two times higher than the one obtained with laminar injection.

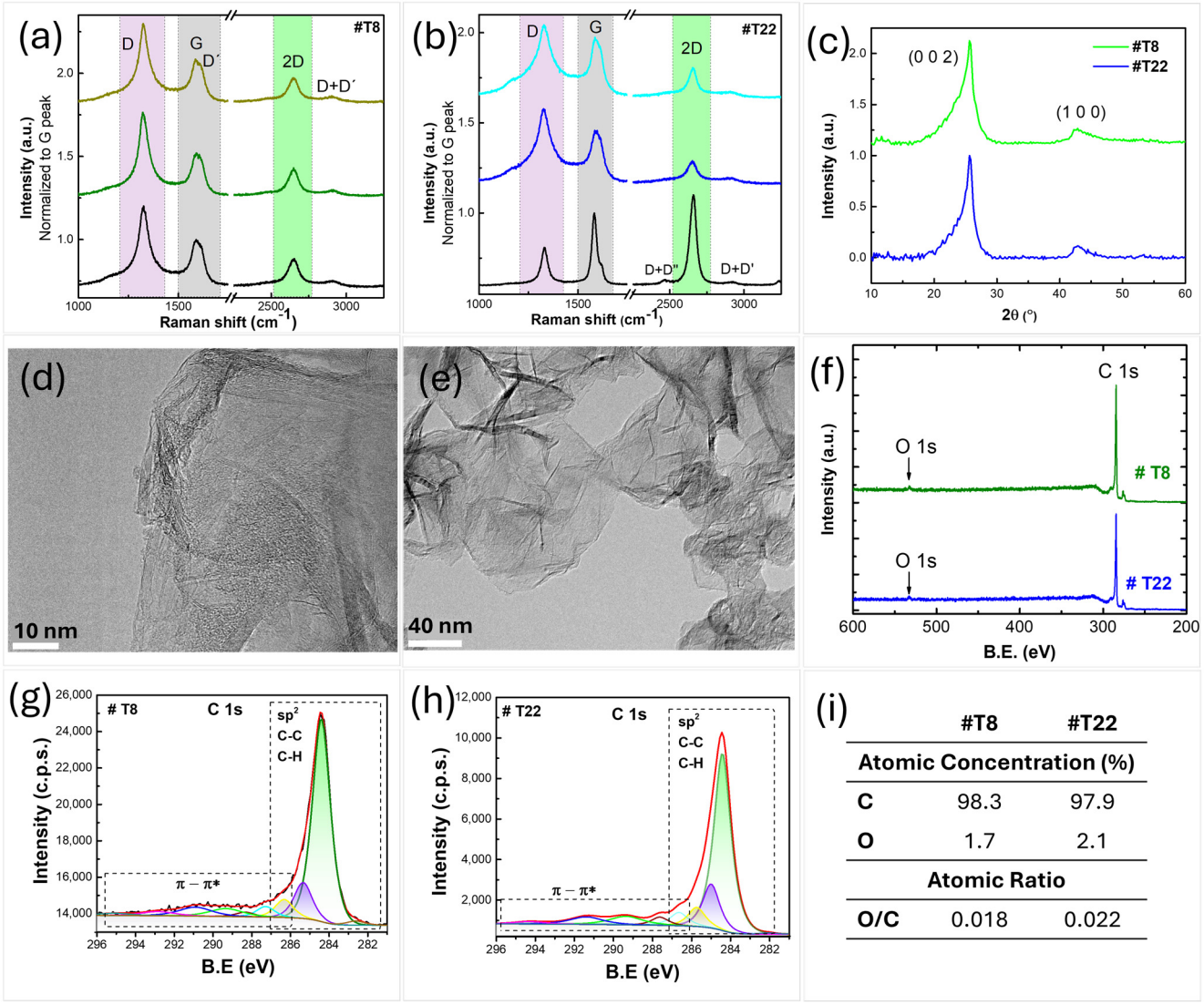

	#T8	#T22
Atomic Concentration (%)		
C	98.3	97.9
O	1.7	2.1
Atomic Ratio		
O/C	0.018	0.022

Figure 4. (**a**,**b**) Raman spectra, (**c**) XRD patterns, (**d**,**e**) TEM micrographs of #T8 and #T22, (**f**) XPS survey spectra, (**g**,**h**) XPS C 1s regions, (**i**) XPS quantification/atomic concentrations (%), and relevant atomic ratios. Synthesis conditions: #T8 and #T22.

The controllable and continuous fabrication of free-standing pure graphene flakes at a gram scale (15–30 mg/min), using methane as a carbon precursor, was achieved. The laminar injection of the background gas promotes the synthesis of graphene sheets with an average lateral size of ~300 nm and an interlayer spacing of 3.42 Å. The high structural quality (with sp^2 carbon atoms ~63% and ~3 at. % of oxygen) was attained. The Raman spectroscopy analysis attests to the fabrication of single- to few-layer graphene sheets and homogeneous samples. The number of monolayers in graphene is controlled by adjusting the methane flow.

The swirl injection of the background gas benefits the homogeneous synthesis of multilayer graphene sheets and leads to a higher production yield (30 mg/min) with respect to the laminar injection at similar plasma conditions. The chemical analysis indicates a very low relative amount of oxygen impurities ~2 at%. Nearly 100% of the conversion efficiency of the carbon precursors was demonstrated in both cases, obtaining as by-products mainly valuable syngas (H_2 and CO) and C_2H_2. The fabricated graphene sheets remain stable over time, as evidenced by the ex situ XPS analyses.

3.3. N-Graphene Synthesis

The plasma synthesis of the N-graphene sheets using methane as a carbon precursor and methylamine as both carbon/nitrogen precursors was performed. Both of the precursors were injected in the "hot" plasma zone by applying top-down injection configuration and laminar flow regime of the background gas (Figure 1). The following plasma synthesis conditions were applied: Q_{Ar} = 5.4 slm, $Q_{Ar'}$ = 2 slm, Q_{CH4} = 150 sccm, Q_{Methyl} = 6 sccm, and P = 5.1 kW.

The HRTEM analysis of the produced N-graphene structures shows the presence of monolayer and multilayer graphene sheets, which is supported by the respective Raman analyses (Figure 5a,c,d). The fingerprint of the graphene-based structures in the Raman spectra 2D peak is detected at 2660 cm^{-1} (Figure 5a). The other two characteristic features of graphitic structures, i.e., the D- and G-bands, are also present. By comparing the present Raman spectra (Figure 5a) with the Raman spectra of the pure graphene sheets synthesized with methane and laminar background injection (Figure 3a), an increase in the D to G intensity ratio (from ~0.51 to ~2.15) and 2D line broadening can be seen. Doping with heteroatoms represents the introduction of structural defects into the graphene lattice; thus, an increase in disorder-related D and D′ peaks is expected. The lowest D to G intensity ratio and narrow 2D line (the lack of line defects) are indicatives of pure graphene [34]. The Raman spectra taken from the different spots of the sample demonstrate homogeneous doping and the presence of multilayer N-graphene sheets.

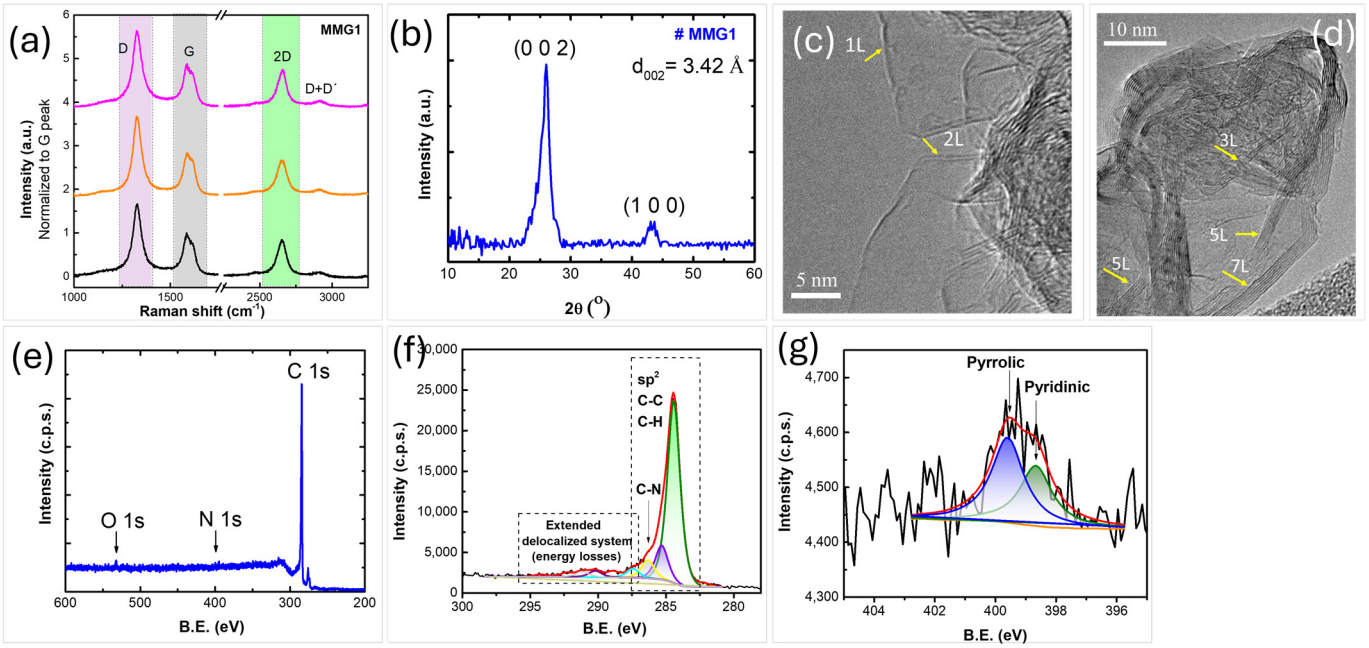

Figure 5. (**a**) Raman spectra collected from different locations, (**b**) the XRD pattern, (**c**,**d**) the TEM micrographs, (**e**–**g**) the XPS survey, and the C 1s, and N 1s regions, respectively, detected from the N-graphene synthesized with methane/methylamine in the top-down injection.

The XRD pattern shows a well-defined (002) plane at 2θ~26.04°, corresponding to an estimated interlayer distance of ~3.42 Å (Figure 5b). The chemical composition of the as-synthesized structures, identified by the XPS analysis, reveals a doping level of ~0.71 at.% of nitrogen, with an oxidation level of ~2 at. % (C/O = 46.7) (Figure 5e–g). The relatively high content of sp^2 carbon atoms = 67% (sp^2 % = $C_{sp2}/C_{Total\ area} \times 100$) attests that the planar structures are preserved during the synthesis process with the injection of the N-precursor in the plasma reactor. Pyridinic, at 398.6 ± 0.2 eV (41.4%), and pyrrolic (and/or nitrile), at 399.6 ± 0.2 eV (58.6%), nitrogen are the dominant configurations (Figure 5g) [39,40].

To further control the nitrogen doping, a combination of top-down + bottom-up injection of methane/methylamine was applied. The following plasma conditions were applied: top-down Q_{Ar} = 5.4 slm, $Q_{Ar'}$ = 2 slm, Q_{CH4} = 150 sccm, Q_{Methyl} = 6 sccm, and P = 5.1 kW. In addition, argon and methylamine, with flow rates of $Q_{Ar''}$ = 100 sccm and $Q_{Methyl''}$ = 20 sccm, were injected bottom-up in the "mild" plasma zone at z = 18 cm (z is the distance with respect to the launcher position) (Figure 1).

A representative SEM micrograph of the sample considered (Figure 6d) illustrates the characteristic free-standing graphene morphology, consisting of curved ultrafine sheets. Monolayer and multilayer sheets can be seen in the TEM micrograph (Figure 6e). The size distribution of the sheets illustrates predominantly N-graphene flakes with lateral sizes in the 300–500 nm range (Figure 6c).

The corresponding Raman spectra support the above findings, i.e., the main feature of the graphene—the 2D-band confirms the presence of graphene sheets (few- to multilayer graphene). The increased I_D/I_G ratio with respect to the pure graphene indicates the successful doping of nitrogen atoms into the graphene lattice (Figure 6a). The Raman spectra collected from different locations of the same sample differ, thus implying non-homogeneous doping. The XRD analysis of the sample reveals a well-pronounced line (002) at 2θ~25.84°, corresponding to an estimated interlayer distance of 3.45 Å (Figure 6b).

The chemical composition XPS analysis of the sample revealed 97.5 at. % of carbon, 1.85 at. % of oxygen, and 0.69 at. % of nitrogen (Figure 6f). Here, the planar nature of the synthesized N-graphene is preserved during the synthesis process manifested by the relatively high content of sp^2/C_{total} = 66% (Figure 6g). The injection of an additional nitrogen precursor (bottom-up methylamine) did not change the doping level with respect to N-graphene sample produced with only the top-down injection of methane/methylamine. However, this modification reduced the oxidation level from 2.08 to 1.85 at.% (C/O = 52.6), and, most importantly, changed the nitrogen doping configurations. The N 1s spectral region was fitted with four main contributions, attributed to pyridinic at 398.6 ± 0.2 eV (20.3%) and 399.2 ± 0.2 eV (35%), pyrrolic (or N in an amine group, having an electron acceptor character) at 400.2 ± 0.2 eV (28.2%), and a smaller contribution of graphitic nitrogen at 401.4 ± 0.2 eV (16.5%) [41]. The peak at the lower B.E. has also been attributed to nitrogen in piperidine-like units [40].

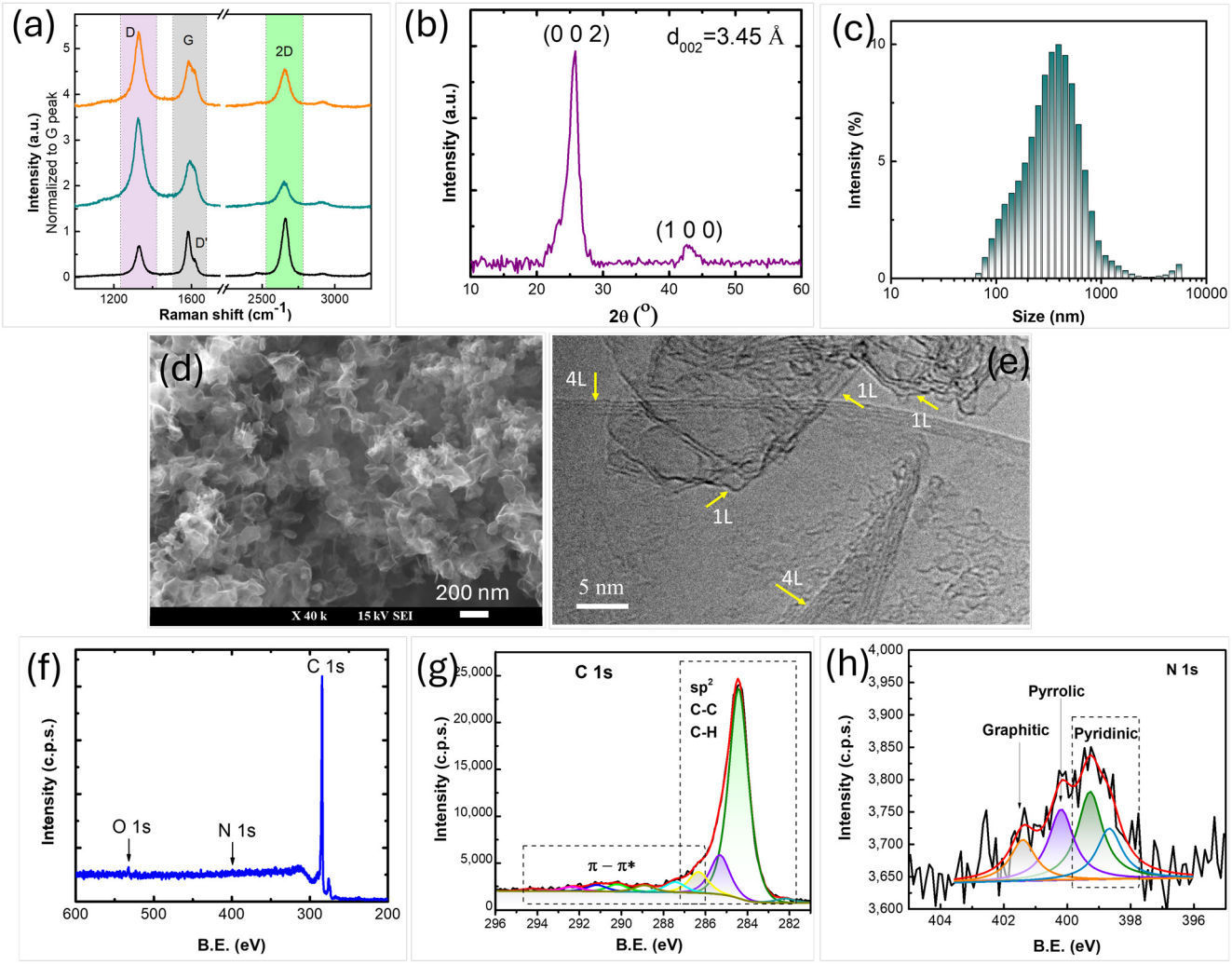

Figure 6. (**a**) Raman spectra collected from different locations, (**b**) the XRD pattern, (**c**) the particle size distribution, (**d**) the SEM and (**e**) TEM micrographs, and (**f**–**h**) the survey of the XPS spectrum, the C 1s region, and the N 1s region, respectively, from the N-graphene synthesized with methane/methylamine in the top-down injection + bottom-up methylamine.

4. Conclusions

The developed plasma process and the corresponding prototype demonstrate the effectiveness and versatility to selectively fabricate graphene and N-graphene at a single step and atmospheric pressure. Using methane/methylamine precursors, protocols for the controllable and continuous fabrication at a gram scale of free-standing graphene/N-graphene have been established. High-structural-quality graphene (with a low oxygen content, a high relative amount of sp^2 carbon, single to few layers, and a ~300 nm lateral size) was synthesized at specific conditions and a relatively high production yield (~15 mg/min) in a stable and reproducible manner. Adjusting the flow regime of the background gas, i.e., from laminar to swirl flow injection, changes the chemical composition of the graphene (lower oxygen) and leads to a 2-fold increase in the production yield (~30 mg/min). Moreover, N-graphene with a doping level of 0.7 at. % N, high sp^2 carbon at ~66%, and an interlayer distance of ~3.42 Å was produced with methane/methylamine using the same plasma reactor. To control the nitrogen doping configuration, the N-precursor was additionally injected into the "mild" plasma environment to meet the growing N-graphene sheets. Few- to multilayer N-graphene flakes with sizes of 300–500 nm were fabricated by applying bottom-up methylamine injection. The same levels of nitrogen doping (~0.7 at. %), at-

tributed to pyridinic, pyrrolic, and a smaller contribution of graphitic nitrogen, and a lower oxidation level (~1.85 at. O %), were achieved with respect to the N-graphene produced by applying top-down injection only. The conversion efficiency of the carbon and nitrogen precursors in the plasma environment was nearly 100%, obtaining as by-products mainly valuable syngas (H_2 and CO) and C_2H_2. Providing stable plasma experimental conditions ensured the quality consistency of the final product and the reproducibility of the process.

Author Contributions: Conceptualization, E.T.; methodology, N.B.; validation, N.B., E.F. and A.D; formal analysis, A.M.F., A.M.B.d.R., M.A., J.K., J.Z., U.C. and A.A.; investigation, N.B., E.F. and A.D.; data curation, N.B., E.F. and A.D.; writing—original draft preparation, N.B.; supervision, E.T.; funding acquisition, L.L.A. and B.G. All authors have read and agreed to the published version of the manuscript.

Funding: This research was funded by the European Union's Horizon research and innovation program under grant agreement No. 766894 through PEGASUS (Plasma Enabled and Graphene Allowed Synthesis of Unique nano-Structures) project; partially by the Portuguese FCT-Fundação para a Ciência e a Tecnologia through the Eager project (PTDC/NAN-MAT/30565/2017). M.A. and J.K. thank the European Union-Next Generation EU, through the National Recovery and Resilience Plan of the Republic of Bulgaria, project. No. BG-RRP-2.004-0008-C01, and INFRAMAT (National Roadmap for Research Infrastructure), supported by Bulgarian Ministry of Education and Science. The work was partially funded by the Portuguese FCT—Fundação para a Ciência e a Tecnologia, through projects UIDB/50010/2020 (https://doi.org/10.54499/UIDB/50010/2020) and UIDP/50010/2020 (https://doi.org/10.54499/UIDP/50010/2020), LA/P/0061/2020 (https://doi.org/10.54499/LA/P/0061/2020); iBB projects UIDB/04565/2020 and UIDP/04565/2020; the i4HB project LA/P/0140/2020, and Centro de Química Estrutural Research through projects UIDB/00100/2020 and UIDP/00100/2020, and the Institute of Molecular Sciences, Associate Laboratory, through project LA/P/0056/2020. U.C. and J.Z. acknowledge the Slovenian Research Agency (ARIS) for the projects Z2-4467 and J2-50074, and program No. P1-0417, as well as the EU Graphene Flagship FLAG-ERA III JTC 2021 project VEGA (PR-11938) and M-ERA.NET 3 project ANGSTROM (the project is funded by the Ministrstvo za visoko šolstvo, znanost in inovacije—MVZI, Slovenia). The authors would like to acknowledge the financial support from the European Innovation Council Pathfinder project under grant agreement No. 101046835.

Data Availability Statement: Data will be made available on request.

Conflicts of Interest: The authors declare no conflicts of interest.

References

1. Urade, A.R.; Lahiri, I.; Suresh, K.S. Graphene Properties, Synthesis and Applications: A. Review. *JOM J. Miner. Met. Mater. Soc.* **2023**, *75*, 614–630. [CrossRef]
2. Mbayachi, V.B.; Ndayiragije, E.; Sammani, T.; Taj, S.; Mbuta, E.R. Graphene synthesis, characterization and its applications: A review. *Results Chem.* **2021**, *3*, 100163. [CrossRef]
3. Sakib, N.; Iqbal, A.P.; Nuruzzaman, D.M. Graphene-based nanocomposites and their fabrication, mechanical properties and applications. *Materialia* **2020**, *12*, 100815. [CrossRef]
4. Yi, M.; Shen, Z. A review on mechanical exfoliation for the scalable production of graphene. *J. Mater. Chem. A* **2015**, *3*, 11700–11715. [CrossRef]
5. Islam, A.; Mukherjee, B.; Pandey, K.K.; Keshri, A.K. Ultra-Fast, Chemical-Free, Mass Production of High Quality Exfoliated Graphene. *ACS Nano* **2021**, *15*, 1775. [CrossRef] [PubMed]
6. Hernandez, Y.; Nicolosi, V.; Lotya, M.; Blighe, F.M.; Sun, Z.; De, S.; McGovern, I.T.; Holland, B.; Byrne, M.; Gun'Ko, Y.K.; et al. High-yield production of graphene by liquid-phase exfoliation of graphite. *Nat. Nanotechnol.* **2008**, *3*, 563–568. [CrossRef]
7. Wang, X.; Sun, G.; Routh, P.; Kim, D.-H.; Huang, W. Heteroatom-doped graphene materials: Syntheses, properties and applications. *Chem. Soc. Rev.* **2014**, *43*, 7067. [CrossRef]
8. Wang, H.; Maiyalagan, T.; Wang, X. Review on recent progress in nitrogen-doped graphene: Synthesis, characterization, and its potential applications. *ACS Catal.* **2012**, *2*, 781–794. [CrossRef]

9. Ito, Y.; Christodoulou, C.; Nardi, M.V.; Koch, N.; Sachdev, H.; Müllen, K. Chemical vapour deposition of N-doped graphene and carbon films. The role of precursors and gas phase. *ACS Nano* **2014**, *8*, 3337–3346. [CrossRef]
10. Dato, A. Graphene synthesized in atmospheric plasmas-A review. *J. Mater. Res.* **2019**, *34*, 214–230. [CrossRef]
11. Pei, S.; Wei, Q.; Huang, K.; Cheng, H.M.; Ren, W. Green synthesis of graphene oxide by seconds timescale water electrolytic oxidation. *Nat. Commun.* **2018**, *9*, 145. [CrossRef]
12. Dong, L.; Chen, Z.; Zhao, X.; Ma, J.; Lin, S.; Li, M.; Bao, Y.; Chu, L.; Leng, K.; Lu, H.; et al. A non-dispersion strategy for large-scale production of ultra-high concentration graphene slurries in water. *Nat. Commun.* **2018**, *9*, 76. [CrossRef] [PubMed]
13. Luong, D.X.; Bets, K.V.; Algozeeb, W.A.; Stanford, M.G.; Kittrell, C.; Chen, W.; Salvatierra, R.V.; Ren, M.; McHugh, E.A.; Advincula, P.A.; et al. Gram-scale bottom-up flash graphene synthesis. *Nature* **2020**, *577*, 647–651. [CrossRef] [PubMed]
14. Dato, A.; Radmilovic, V.; Lee, Z.; Phillips, J.; Frenklach, M. Substrate-free gas-phase synthesis of graphene sheets. *Nano Lett.* **2008**, *8*, 2012–2016. [CrossRef] [PubMed]
15. Tatarova, E.; Dias, A.; Henriques, J.; Abrashev, M.; Bundaleska, N.; Kovacevic, E.; Bundaleski, N.; Cvelbar, U.; Valcheva, E.; Arnaudov, B.; et al. Towards large-scale in free-standing graphene and N-graphene sheets. *Sci. Rep.* **2017**, *7*, 10175. [CrossRef]
16. Tsyganov, D.; Bundaleska, N.; Tatarova, E.; Dias, A.; Henriques, J.; Rego, A.; Ferraria, A.; Abrashev, M.V.; Dias, F.M.; Luhrs, C.C.; et al. On the plasma based growth of "flowing" graphene sheets at atmospheric pressure conditions. *Plasma Sources Sci. Technol.* **2016**, *25*, 015013. [CrossRef]
17. Rincón, R.; Melero, C.; Jiménez, M.; Calzada, M.D. Synthesis of multi-layer graphene and multi-wall carbon nanotubes from direct decomposition of ethanol by microwave plasma without using metal catalysts. *Plasma. Sources Sci. Technol.* **2015**, *24*, 032005. [CrossRef]
18. Melero, C.; Rincón, R.; Muñoz, J.; Zhang, G.; Sun, S.; Perez, A.; Royuela, O.; González-Gago, C.; Calzada, M.D. Scalable graphene production from ethanol decomposition by microwave argon plasma torch. *Plasma Phys. Control Fusion.* **2018**, *60*, 014009. [CrossRef]
19. Casanova, A.; Rincón, R.; Muñoz, J.; Ania, C.O.; Calzada, M.D. Optimizing high-quality graphene nanoflakes production through organic (bio)-precursor plasma decomposition. *Fuel Process Technol.* **2021**, *212*, 106630. [CrossRef]
20. Münzer, A.; Xiao, L.; Sehlleier, Y.H.; Schulz, C.; Wiggers, H. All gas-phase synthesis of graphene: Characterization and its utilization for silicon-based lithium-ion batteries. *Electrochim. Acta* **2018**, *272*, 52. [CrossRef]
21. Fortugno, P.; Musikhin, S.; Shi, X.; Wang, H.; Wiggers, H.; Schulz, C. Synthesis of freestanding few-layer graphene in microwave plasma: The role of oxygen. *Carbon* **2022**, *186*, 560–573. [CrossRef]
22. Zafar, M.A.; Jacob, M.V. Plasma-based synthesis of graphene and applications:a focused review. *Rev. Mod. Plasma Phys.* **2022**, *6*, 37. [CrossRef]
23. Toman, J.; Jašek, O.; Šnírer, M.; Pavliňák, D.; Navrátil, Z.; Jurmanová, J.; Chudják, S.; Krčma, F.; Kudrle, V.; Michalička, J. On the transition of reaction pathway during microwave plasma gas-phase synthesis of graphene nanosheets: From amorphous to highly crystalline structure. *Plasma Process Polym.* **2021**, *18*, 2100008. [CrossRef]
24. Zafar, M.A.; Jacob, M.V. Synthesis of free-standing graphene in atmospheric pressure microwave plasma for the oil-water separation application. *Appl. Surf. Sci. Adv.* **2022**, *11*, 100312. [CrossRef]
25. Zafar, M.A.; Varghese, O.K.; Hernandez, F.C.R.; Liu, Y.; Jacob, M.V. Single-step synthesis of nitrogen-doped graphene oxide from aniline at ambient conditions. *ACS Appl. Mater. Interfaces* **2022**, *14*, 5797–5806. [CrossRef]
26. López-Cámara, C.-F.; Fortugno, P.; Asif, M.; Musikhin, S.; Prindler, C.; Wiggers, H.; Endres, T.; Eaves, N.; Daun, K.J.; Schulz, C. Evolution of particle size and morphology in plasma synthesis of few-layer graphene and soot. *Combust. Flame* **2023**, *258*, 112713. [CrossRef]
27. Terasawa, T.; Saiki, K. Synthesis of nitrogen-doped graphene by plasma enhanced chemical vapor deposition. *Japanese J. Appl.Phys.* **2012**, *51*, 055101. [CrossRef]
28. Kumar, A.; Voevodin, A.; Paul, R.; Altfeder, I.; Zemlyanov, D.; Zakharov, D.; Fisher, T. Nitogen-doped graphene by microwave plasma chemical vapor deposition. *Thin Solid Films* **2013**, *528*, 269–273. [CrossRef]
29. Wei, D.; Peng, L.; Li, M.; Mao, H.; Niu, T.; Han, C.; Chen, W.; Wee, A.T.S. Low temperature critical growth of high quality nitrogen doped graphene on dielectrics by plasma enhanced chemical vapor deposition. *ACS Nano* **2015**, *9*, 164–171. Available online: https://pubs.acs.org/doi/10.1021/nn505214f (accessed on 5 May 2023). [CrossRef] [PubMed]
30. Ahmed, S.; Ali, A.; Asif, M.; Shim, J.; Park, G. Exploring innovative trends and advancements in rechargeable zinc-air batteries. *Inorg. Chem. Commun.* **2024**, *170*, 113288. [CrossRef]
31. Dias, A.; Bundaleska, N.; Felizardo, E.; Tsyganov, D.; Almeida, A.; Ferraria, A.; Rego, A.B.D.; Abrashev, M.; Strunskus, T.; Santhosh, N.; et al. N-Graphene-Metal-oxide(sulfide) Hybrid Nanostructures: Single-Step Plasma-Enabled Approach for Energy Storage Applications. *Chem. Eng. J.* **2021**, *430*, 133153. [CrossRef]
32. Dias, A.; Felizardo, E.; Bundaleska, N.; Abrashev, M.; Kissovski, J.; Ferraria, A.M.; Rego, A.M.; Strunskus, T.; Carvalho, P.A.; Almeida, A.; et al. Plasma-enabled multifunctional platform for gram-scale production of graphene and derivatives. *Appl. Mat. Today* **2024**, *36*, 102056. [CrossRef]

33. Bundaleska, N.; Tsyganov, D.; Dias, A.; Felizardo, E.; Henriques, J.; Dias, F.M.; Abrashev, M.; Kissovski, J.; Tatarova, E. Microwave plasma enabled synthesis of free standing carbon nanostructures at atmospheric pressure conditions. *Phys. Chem. Chem. Phys.* **2018**, *20*, 13810. [CrossRef]
34. Bundaleska, N.; Henriques, J.; Abrashev, M.; Botelho do Rego, A.M.; Ferraria, A.M.; Almeida, A.; Dias, F.M.; Valcheva, E.; Arnaudov, B.; Upadhyay, K.K.; et al. Large-scale synthesis of freestanding N-doped graphene using microwave plasma. *Sci. Rep.* **2018**, *8*, 12595. [CrossRef]
35. Bundaleska, N. Prospects for microwave plasma synthesized N-graphene in secondary electron emission mitigation applications. *Sci. Rep.* **2020**, *10*, 13013. [CrossRef] [PubMed]
36. Moisan, M.; Zakrzewski, Z. Plasma sources based on the propagation of electromagnetic surface waves. *J. Phys. D Appl. Phys.* **1991**, *24*, 1025. [CrossRef]
37. Campos, J.M.; Ferraria, A.M.; Botelho do Rego, A.M.; Rosário Ribeiro, M.; Barros-Timmons, A. Studies on PLA grafting onto graphene oxide and its effect on the ensuing composite films. *Mater. Chem. Phys.* **2015**, *166*, 122–132. [CrossRef]
38. Li, Z.; Lu, C.; Xia, Z.; Zhou, Y.; Luo, Z. X-ray diffraction patterns of graphite and turbostratic carbon. *Carbon* **2007**, *45*, 1686–1695. [CrossRef]
39. Beamson, G.; Briggs, D. High Resolution XPS of Organic Polymers. In *The Scienta ESCA300 Database*; John Wiley & Sons: New York, NY, USA, 1992.
40. Naumkin, A.V.; Kraut-Vass, A.; Gaarenstroom, S.W.; Powell, C.J. *NIST X-ray Photoelectron Spectroscopy (XPS) Database*, version 4.1. NIST Standard Reference Database 20. NIST: Gaithersburg, MD, USA, 2012. [CrossRef]
41. Kato, T.; Yamada, Y.; Nishikawa, Y.; Otomo, T.; Sato, H.; Sato, S. Origins of peaks of graphitic and pyrrolic nitrogen in N1s X-ray photoelectron spectra of carbon materials: Quaternary nitrogen, tertiary amine, or secondary amine? *J. Mater. Sci.* **2021**, *56*, 15798–15811. [CrossRef]